Journal of Solid State Chemistry 322 (2023) 124003

Contents lists available at ScienceDirect

Journal of Solid State Chemistry

journal homepage: www.elsevier.com/locate/jssc

Study of mechanical, optical and transport aspirants of double perovskites Cs_2XInI_6 (X = Li, Na) for solar cells and clean energy applications

Tariq M. Al-Daraghmeh [a], Omar Zayed [a], Taharh Zelai [b], Sadaf Saba [c], Ghulam M. Mustafa [d,*], Othman Hakami [e], Hind Albalawi [f,**], S. Bouzgarrou [g,h], Z. Mahmoud [i], Q. Mahmood [j,k]

[a] Basic Sciences Department, King Abdullah II School of Engineering, Princess Sumaya University for Technology, P.O.Box 1438, Al-Jubaiha, 11941, Amman, Jordan
[b] Department of Physics, Faculty of Science, Jazan University, Jazan, Saudi Arabia
[c] Computational Materials Modeling Laboratory, Department of Physics, Government College University, Faisalabad, 38040, Pakistan
[d] Department of Physics, Division of Science & Technology, University of Education Lahore, Pakistan
[e] Department of Chemistry, Faculty of Science, Jazan University, Jazan, Saudi Arabia
[f] Department of Physics, College of Sciences, Princess Nourah bint Abdulrahman University (PNU), P.O. Box 84428, Riyadh, 11671, Saudi Arabia
[g] Department of Physics, College of Science, Qassim University, P. O. 64, Buraidah, Saudi Arabia
[h] Laboratoire de Microélectronique et Instrumentation (UR 03/13-04), Faculté des Sciences de Monastir, Avenue de l'Environnement, 5000, Monastir, Tunisia
[i] Departement of Physics, College of Sciences, King Khalid University, P.O. Box 9004, Abha, Saudi Arabia
[j] Basic and Applied Scientific Research Center, Imam Abdulrahman Bin Faisal University, P.O. Box 1982, Dammam, 31441, Saudi Arabia
[k] Department of Physics, College of Science, Imam Abdulrahman Bin Faisal University, P.O. Box 1982, Dammam, 31441, Saudi Arabia

A B S T R A C T

The double perovskites (DPs) are extensively explored materials owing to their potential for optoelectronic and thermoelectric devices. In current report, the density functional theory-based Wien2k code is utilized to check the electrical, mechanical, optical, and thermoelectric characteristics of Cs_2XInI_6 (X = Li, Na). The calculation of enthalpy of formation yields information about the thermodynamic stability, while computing the tolerance factor yields information about the structural durability. Elastic constant dependent, moduli of elasticity have been computed which confirm the ductile nature of Cs_2LiInI_6 and brittle nature of Cs_2NaInI_6. Utilizing modified Beck and Johnson potential (TB-mBJ) to measure the band structures and optical characteristics reveals the bandgaps of 1.23, and 1.64 eV for Li and Na-based DPs, respectively. Additionally, the optical behavior is elaborated by computing refractive index, dielectric constant and reflectivity. The broad absorption bands in visible range increases their potential for solar cells. BoltzTrap code is utilized to compute temperature-dependent transport parameters. The capability of these DPs for thermoelectric applications is determined by figure of merit in the range of 200–800 K.

1. Introduction

Coal, gas, and other nonrenewable energy sources are rapidly running out and are predicted to be depleted by the end of 2050 [1]. Researchers are exploring new ways to innovate technologies for obtaining energy from renewable sources to meet the rising need and scarcity of energy in the modern era [2–5]. In this perspective, waste heat and sunlight are regarded as capable substitutes for conventional energy sources like fossil fuels. Solar cell technology distinguishes out from other existing renewable energy sources due to its low production costs and great efficiency. Any material's ability to convert energy is analyzed during solar cell manufacturing, so this aspect is significant for solar cell technology. However, designing an effective, functional, and economical solar cell, demands ongoing scientific research. In the development of the photovoltaic industry, lead-based perovskite solar cells reveal the highest efficiency [6]. They have a remarkable capacity for absorbing visible energy, which suggests potential solar cell uses [7–10]. In the optoelectronic field, these materials have been used since 2009, when their conversion efficiency was 3.8% [11], it has since miraculously improved to more than 25.2% [12]. However, several challenges prevent extensive commercialization of these compositions including the toxicity of lead-based perovskites and their low stability [13]. The influence of moisture on the efficiency of perovskite solar cells has also been studied [14,15]. Therefore the photovoltaic industry is looking for a potential lead-free substitute that should be non-toxic, highly stable, and efficient. In this regard, lead-free double perovskites with high compositional range, stable and suitable bandgap is emerging as a new candidate for the photovoltaic industry [16,17].

The formula for double perovskite is generally written as $A_2B'B''X_6$, where A is a bigger-sized cation that typically comes from an alkali metal

* Corresponding author.
** Corresponding author.
E-mail addresses: gmmustafa25@gmail.com (G.M. Mustafa), HMALbalawi@pnu.edu.sa (H. Albalawi).

https://doi.org/10.1016/j.jssc.2023.124003
Received 19 January 2023; Received in revised form 15 March 2023; Accepted 22 March 2023
Available online 23 March 2023

group, such as Cs, Rb, whereas X is a halide ion and B' and B'' are monovalent (B' = silver, copper, sodium), trivalent (B'' = indium, bismuth) cations, and [18]. There have been several experimental and theoretical investigations to determine if cation order and vacancy order double perovskites (DPs) are suitable for optoelectronic and photovoltaic industries [19]. For example, Slavery et al. fabricated $Cs_2AgBiBr_6$ double perovskite and investigated its optoelectronic characteristics, suggesting that both hybrid and inorganic configurations have interesting prospects for photovoltaic and optoelectronic uses and must be investigated further [20]. Although this formulation has an appropriate bandgap value with indirect bandgap character. Additionally, Volonakis et al. conducted experimental and theoretical research on $Cs_2InAgCl_6$ double perovskite and reported a direct bandgap of 3.3 eV. They suggested that the bandgap of such a composition can also be modified by combining the halides [21]. According to Kangsabaniket et al. who conducted an inductive investigation, double perovskites are replacing simple perovskites because of their greater stability and superior energy conversion efficiency [22]. A comprehensive study was conducted by Chakra-borty et al. about how to twice the stability and scalability of perovskites to expand their utility in solar cell and photovoltaic applications [23]. Geisz et al. established a new record by obtaining the efficiency of the solar cell at about 47.1%. This efficiency rate is 11.1% higher than the thin-film solar cell value that has previously been reported [24].

This literature overview showed that double perovskite halides have substantial thermal and mechanical stability, however, their wide, indirect bandgap prevents them from being used in photovoltaic devices [25]. The wide band gap DPs $Cs_2NaInCl_6$ nanocrystals doped with Tb^{3+} emits intense beans of visible and extensively used for light emitting diods. Chen et al., also explored $Cs_2NaInCl_6$ with doping of Mn^{2+} ions to control the photoluminese propertis [26,27]. Furthermore, Zhou et al., also worked in this direction by doping of Sb^{3+}/Bi^{3+} in $Cs_2NaInCl_6$ for solid state lightning. Through photoluminese and DFT appraoch, the 77% quantum yield of yellow and blue emission had been noticed which increase their potential for solar cell industry [28]. Shuai et al., elaborated the optical and electronic characteristics of $Cs_2Na(Sb/Bi)X_6$ (X = halogens) for energy harvesting applications [29,30]. The light of above discussion, it is essential to use a trustworthy DFT methodology to calculate the Boltzmann transport properties and complex dielectric feature of Cs_2LiInI_6 and Cs_2NaInI_6 which will support the practical uses of these DPs. The drawbacks of halides and advantages of oxides materials have been illustrated in detail in the revised manuscript where it revealed quite stable response temperature, oxygen, electromagnetic radiation and oxide compounds [31–36]. The studied compounds are double perovskites halides which do not have oxygen. However, in practical realization of these materials the vacuum is necessary because the open sintering will carry the oxygen [37,38]. The atomic positions of Li+ and Na + doping cations in the initial Cs_2XInI_6 unit cell have been discussed in detail. Using the Rietveld method, the confirmation of atomic positions can be done by X-ray or neutron diffraction spectra [39–42].

The literature on the studied DPs Cs_2LiInI_6, and Cs_2NaInI_6 is very limited, however, the related compounds of these DPs family are studied by different researchers. The structural, optical, and mechanical parameters of $Cs_2LiInBr_6$ has been calculated. The elastic constants C_{11} = 25, C_{12} = 11, C_{44} = 10 confirmed the mechanical stability with Poisson's ratio of 0.26 which assured their ductile nature [43,44]. Furthermore, in their study, Manzoor et al., observed the bangap values of .90 and 1.66 eV with figure of merits 0.43, and 0.50 for Rb_2LiTlX_6 (X = Cl or Br) [45]. Iqbal et al., reported narrow band gaps 1.05, 0.65, and 0.25 eV of Rb_2AlInX_6 (X = Cl, Br, I) and ZT values ranging from 0.75 to 0.77 [46]. As far as we know, the electrical, thermoelectric, and optical characteristics of the Cs_2XInI_6 (X = Li, Na) have not yet been investigated thoroughly. For this, we have used the DFT approach to analyze electronic and optical characteristics by Tran-Balaha modified Becke-Jhonson potential functional (TB-mBJ). In addition, BoltzTrap code was used to comprehend the transport behavior of these compositions. We expect that the finding of the investigation of optoelectronic and thermoelectric properties of Cs_2XInI_6 (X = Li, Na) will be a healthy addition in the existing body of knowledge regarding DPs and will inspire experimental and theoretical researchers to explore the potential DPs for viable light applications in photovoltaic and thermoelectric technology.

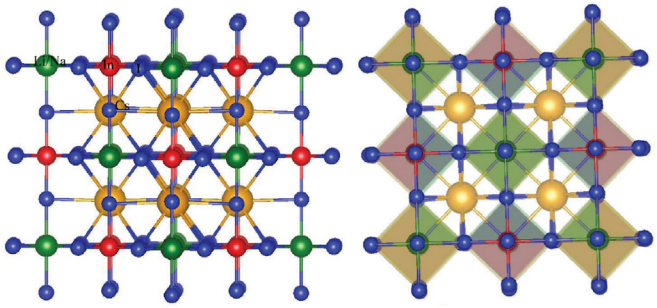

Fig. 1. Unit cell of Cs_2XInI_6 (X = Li, Na) double perovskites ball stick model (left) and polyhedral model (right) [Cs balls (Brown color), Li/Na balls (Green color), In balls (Red color), I balls (Blue color)].

2. Computational method

By using the full potential linearized augmented plane wave method (FP-LAPW) integrated into the WIEN2k code, structural, thermoelectric, and optoelectronic characteristics of Cs_2XInI_6 (X = Li, Na) were calculated [47,48]. The Pardew Burke Ernzerhof Generalized Gradient Approximation (PBE-GGA) is a correlation and exchange perspective employed in this investigation because it provides extremely accurate estimates of all ground state parameters except bandgap, which is understated [49]. The updated TB-mBJ was incorporated to address this underestimate. The TB-mBJ is most versatile potential for precise calculation of electronic properties and band gaps of semiconductor materials. The Accuracy of hybrid functional (HSE06) and TB-mBJ are equivalent which were already solved in the literature. The advantage of TB-mBJ is that it has less computational time and easy to operate, therefore, the results are analyzed through TB-mBJ. The semiconductor material's band gap is precisely calculated using the TB-mBJ [50]. Using the following equation, the potential was determined;

$$V_{x,\sigma}^{mBJ}(\mathrm{r}) = \mathrm{c}\, V_{x,\sigma}^{BR}(\mathrm{r}) + (3c-2)\frac{1}{\pi}\frac{\sqrt{5}}{12}\frac{\sqrt{2t_\sigma(\mathrm{r})}}{\rho_\sigma(\mathrm{r})} \quad (1)$$

Here c, ρ_σ, and $t_\sigma(r)$ represents charge convergence factor, the density of states, and kinetic energy respectively. The following expression was used to calculate the charge convergence value;

$$\mathrm{c} = \alpha + \left(\beta\frac{1}{V_{Cell}}\int d^3(\mathrm{r})\frac{|\nabla\rho(\mathrm{r})|}{\rho(\mathrm{r})}\right)^{1/2} \quad (2)$$

Here, the values of α and β are random constants that are modified by WEIN2k. In this calculation, the order of k-mesh was developed as 10 × 10 × 10 where thousand k-points were used and the highest values of angular momentum (L_{max}) were modified to 7 so the mulplication of R_{MT} × K_{max} will become 8, here R_{MT} and K_{max} are the radius of the muffin-tin sphere and cut off wave vectors, respectively. Additionally, a limit of 12 was specified for the maximum Fourier transformation vector [51]. In the self-consistent field (SCF), 0.00001 Ry was chosen as the minimal charge convergence condition. The Birch Murnaghan (BM) relation was employed to optimize energy volume. Transport properties including thermal and electrical conductivities, Seebeck coefficient, power factor, and figure of merit were measured using the Boltz-Trap code [52]. The ShengBTE code has been utilized to compute lattice thermal conductivity [53].

Table 1
The computed factors of Cs_2XInI_6 (X = Li, Na).

Parameters	Cs_2LiInI_6	Cs_2NaInI_6
Lattice constant a_o (Å)	12.02	12.19
enthalpy of formation ΔH (eV)	−0.97	−1.06
Bulk modulus B (Gpa)	16.71	14.30
Tolerance factor t_G	0.92	0.90
Bandgap E_g	1.23	1.64
Zero energy value $\varepsilon_1(0)$	3.81	3.55
Static refractive index n(0)	1.95	1.88
Zero energy value R (0)	0.104	0.094

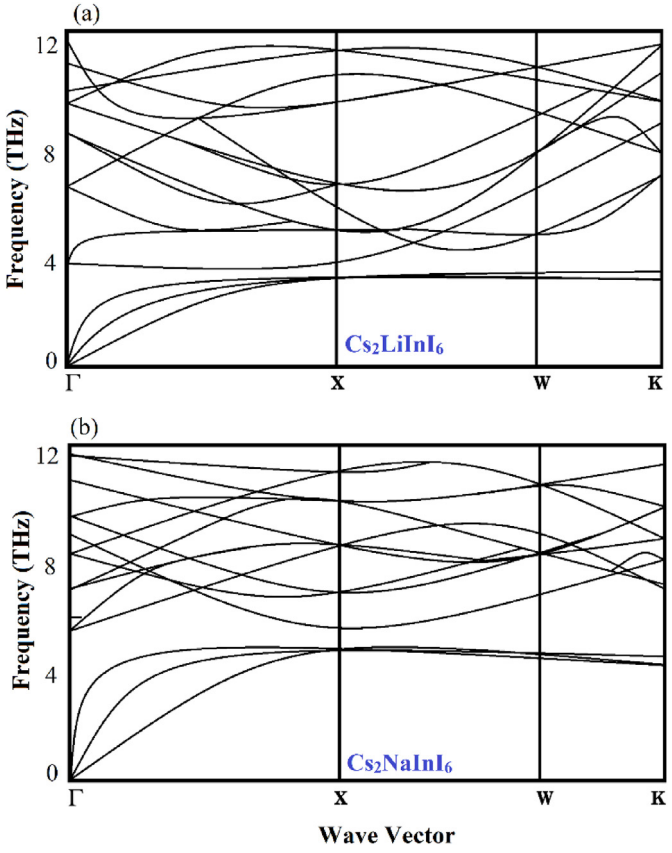

Fig. 2. (a, b) Phonons band structures of (a) Cs_2LiInI_6, and (b) Cs_2NaInI_6.

3. Discussion of results

3.1. Structural characteristics

The unit cell of Cs_2XInI_6 (X = Li, Na) compositions which is a FCC crystal structure having space group *Fm-3m* is illustrated in Fig. 1 [54]. The position of Cs, X, In, and I atoms inside this unit cell is (0.25, 0.25, 0.25), (x, 0, 0), (0, 0, 0), and (0.5, 0.5, 0.5), respectively [55]. The Cs, X, In, and I atoms are represented in this unit cell by yellow, green, red, and blue-colored atoms, respectively. To investigate the ground state structural features of composition under analysis, the PBE-GGA approximation was used.

Table 1 lists computed lattice parameters a_o (Å) and bulk modulus B_o (GPa) for Cs_2LiInI_6 and Cs_2NaInI_6. It is clear that when Li is changed with Na, the values of a_o (Å) raised from 12.02 to 12.19 Å, which is because of increasing ionic radii from 0.76 Å (Li) to 1.02 Å (Na). By replacing Li for Na, the bulk modulus B_o reduces from 16.71 to 14.30 GPa due to the rise in the interatomic distance caused by the rise in cationic size, which produces solids less dense. For a more thorough investigation of thermodynamic stability, the chemical equation given below was used to calculate formation energy.

$$H_f = E_{(Cs_aX_bIn_cI_d)} - (aE_{Cs} + bE_X + cE_{In} + dE_I) \quad (3)$$

Where, $E_{(Cs_aX_bIn_cI_d)}$, E_{Cs}, E_X, E_{In}, and E_I are energies of Cs_2XInI_6, Cs, X, In, and I atoms, correspondingly. In above equation, the coefficeints (a, b, c, and d) represent no. of elements. As seen in Table 1, the difference in energy is also calculated as formation energy (H_f) [56]. The values of H_f for the compositions Cs_2LiInI_6 and Cs_2NaInI_6 were reported to drop from −0.97 to −1.06, respectively. All of these compositions' structural integrity was validated by the endothermic phase disintegration, which is expressed by the negative values of H_f. A significant component that determines the perovskite's structural stability is the Goldsmith tolerance factor (t_F). The value of t_G for stable structures must be between 0.81 and 1.11 [57]. For the current report, the value of t_G was 0.92 for Cs_2LiInI_6 and 0.90 for Cs_2NaInI_6 as given in Table 1.

The phonons spectrum has been obtained though Phonopy code which based on density functional theory perturbation (DFTP) as presented in Fig. 2 (a, b). The unit cells of Cs_2XInI_6 (X = Li, Na) includes of 30 modes but for simple band structures, we have only considered here 15 modes. From these modes 3 acoustic and 12 are optical modes. The optical modes usually have positive frequencies, but the vibration of lattice phonons disturb the acoustic modes to negative frequencies due to which materials becomes unstable. In present case, at Γ symmetry point 3 acoustic phonons modes cancel each other which confirm the dynamical stability of studied structure [58].

3.2. Mechanical characteristics

The mechanical parameters for Cs_2XInI_6 (X = Li, Na) as shown in Table 2. The mechanical response of cubic systems can be determined by calculating the elastic constants C_{11}, C_{12}, and C_{44}. The relation $C_{11} - C_{12} > 0$, $C_{44} > 0$, $C_{11} + 2C_{12} > 0$, and $C_{12} < B_o < C_{11}$ also determine the mechanical stability and named as Born stability criteria [59].

If we proceed from Li to Na, the material lost the capacity to tolerate more changes and becomes less stable because the value of the lattice constant rises and leads to a reduction in the modulus of elasticity's value. Before employing a material to fabricate a device, a deterministic approach is required to determine whether it is brittle or ductile and it is done by calculating the Poisson (ν) and Pugh's ratio (B/G). Any material is tagged as ductile B/G > 1.75 and $\nu > 0.26$ otherwise brittle [60]. The Li-based composition has a B/G value of 2.17, but the value for Na-based composition is 1.63, proving that the Li-based composition is ductile whereas the Na-based composition is brittle. The value of A = 1 demonstrates isotropic behavior, whereas its deviance illustrates its anisotropic nature. According to calculated values listed in Table 2, the Li comprising double perovskite seems to be more isotropic than Na comprising double perovskite. Additionally, using the relationships

Table 2
The elastic and thermodynamic parameters of Cs_2XInI_6 (X = Li, Na).

Parameters	Cs_2LiInI_6	Cs_2NaInI_6
Elastic constant C_{11} (GPa)	21.79	34.25
Elastic constant C_{12} (GPa)	9.24	8.50
Elastic constant C_{44} (GPa)	6.09	9.04
Bulk modulus B (GPa)	13.42	17.0
Shear modulus G (GPa)	6.16	10.42
Young modulus E (GPa)	16.0	25.97
Pugh's ratio B/G	2.17	1.63
Poisson ratio ν	0.30	0.24
Anisotropy A	0.97	0.70
Longitudinal sound velocity V_ℓ (Km/s)	2.2	2.69
Transverse sound velocity V_t (Km/s)	1.18	1.56
Average sound velocity V_m (Km/s)	1.32	1.73
Debye temperature Θ_D (K)	112	144
Melting temperature T_m (K)	682	755
Hardness H_a (GPa)	0.81	1.76
Lattice thermal conductivity K_{min} (W/mK)	0.082	0.101

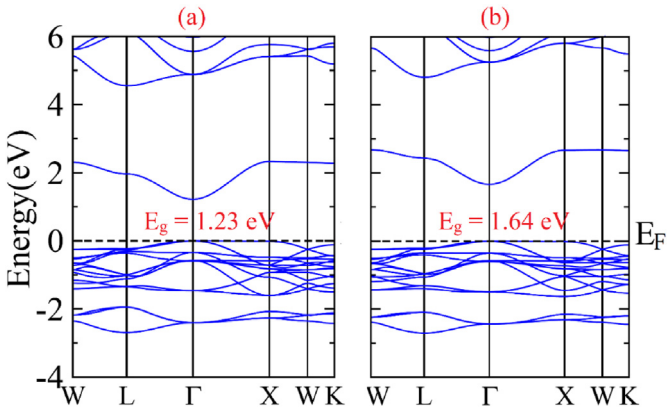

Fig. 3. (a, b): Band structure of (a) Cs_2LiInI_6 and (b) Cs_2NaInI_6 double perovskites.

provided elsewhere [61], the Navier equation is examined to determine the average transverse and longitudinal components of sound velocity v_m. The Debye temperature is dependent on v_m and is calculated using the relation;

$$\theta_D = \frac{h}{k_B}\left[\frac{3nN_A\rho}{4\pi M}\right]^{1/3} v_m \quad (4)$$

Here, constants with distinct values are ρ, M, and N_A. The estimated θ_D is higher for Cs_2NaInI_6 than Cs_2LiInI_6, demonstrating that Na ions double perovskites have a higher lattice vibration sustainability than that of Li ions double perovskites [62]. The elastic constants for directions C_{11} have also been utilized to determine the melting temperature of investigated double perovskites using the given expression;

$$T_m = 553 + 5.91C_{11}/\text{GPa} \quad (5)$$

The calculated T_m values assured that the examined double perovskites can be manufactured at RT. The investigation demonstrates that T_m is higher for Cs_2NaInI_6 than Cs_2LiInI_6. This indicates that Na-based double perovskites have stronger bonds than Li-based double perovskites because Na ions have larger ion sizes. Moreover, the given formula is used to determine the hardness of investigated double perovskites.

$$Hv = 0.92(G/B)^{1.137}\, G^{0.708} \quad (6)$$

The modifications in compound formation and associated directional characteristics that Marathe et al., 2016 [63] observed for cubic structures are avoided by the Hv. Since Cs_2NaInI_6 has a greater shear modulus and stronger bonding, so it is harder than Cs_2LiInI_6, according to values of Hv presented in Table 2. The expression of Cahill criteria is used to extract the lowest lattice conductivity of the analyzed double perovskites to understand lattice dynamics [64,65].

$$k_{min} = \frac{k}{2.48}(n_b)^{\frac{2}{3}}\,(vl + 2v_t) \quad (7)$$

The results of k_{min} are shown in Table 2 which shows extremely fewer values for the examined double perovskites and are in accord with lattice thermal conductivity calculated using ShengBTE code. These double perovskites are therefore remarkable for applications involving renewable energy because of their lower lattice thermal conductivity, light energy absorption in the visible range, and greater ZT.

3.3. Electronic characteristics

The band gap values, carrier mobilities, and carrier concentrations can be used to classify the materials like metals, semiconductors, and insulators. In order to determine whether the materials under examination are metallic or semiconductors, their electronic properties, particularly band structure are evaluated which leads to their specification for numerous applications [66]. The band structure for these two

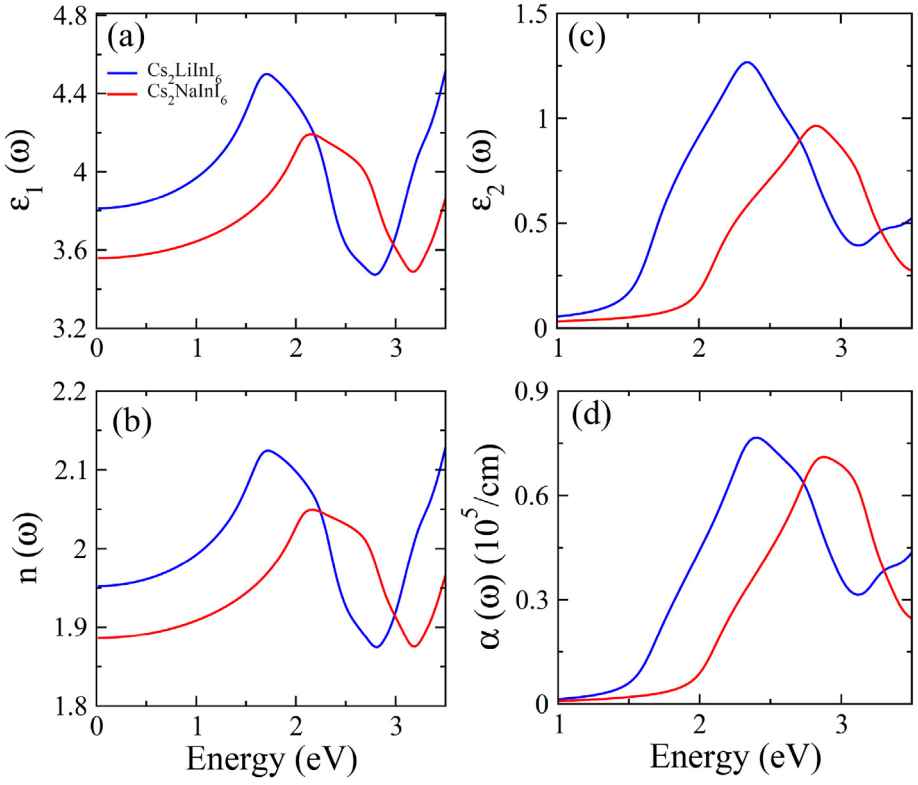

Fig. 4. (a–d): (a) Real part of dielectric constant, (b) refractive index, (c) imaginary part of dielectric constant and (d) absorption coefficient of Cs_2XInI_6 (X = Li, Na) double perovskites.

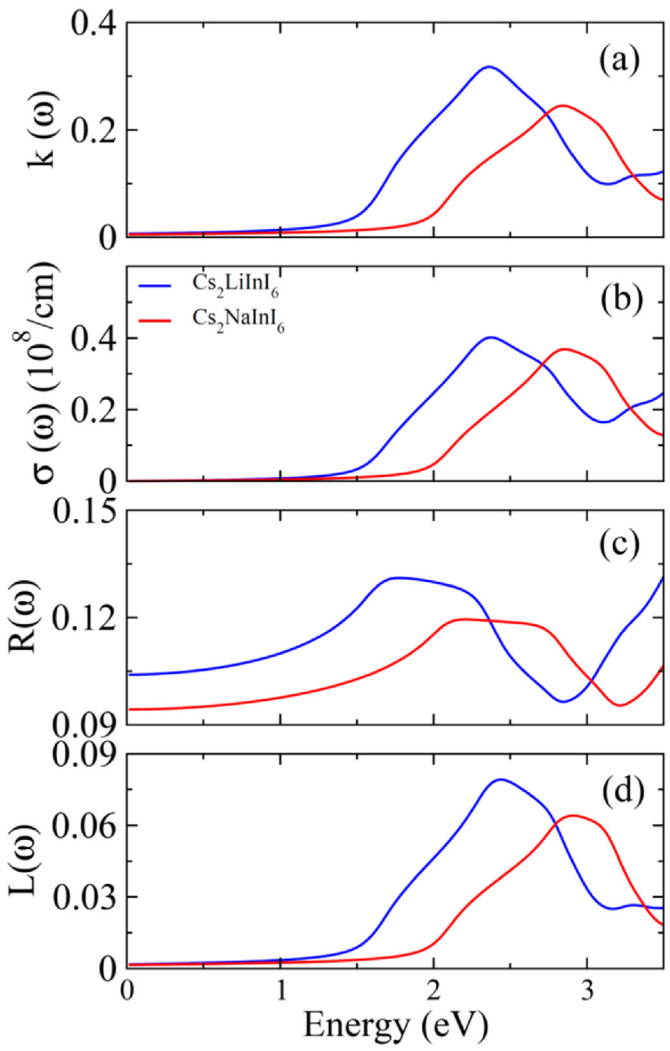

Fig. 5. (a–d): (a) extinction coefficient, (b) optical conductivity, (c) optical reflectivity and (d) optical loss of Cs_2XInI_6 (X = Li, Na) double perovskites.

compositions is represented in Fig. 3 (a, b). The TB-mBJ potential is used to compute these outcomes with accuracy. The bottom of the conduction band and top of the valence bands of these compositions emerged at the same Γ-point in Fig. 3 (a, b), resulting in direct band gaps (E_g) nature and the numerical value of these compositions demonstrate their semiconducting character. The bandgap energy increased as Li is replaced by Na in the composition of Cs_2XInI_6 (X = Li, Na). For the composition, Cs_2LiInI_6, and Cs_2NaInI_6, the bandgap energies were measured to be 1.23 and 1.64 eV, respectively.

3.4. Optical characteristics

The optical characteristics of materials under investigation will depend on how photons of light interact with electron and band gap's nature. The optical characteristics of double perovskites Cs_2XInI_6 (X = Li, Na) are discussed here on the basis of the dielectric constant ε (ω), with a real component of ε_1 (ω) and an imaginary component of ε_2 (ω). The ε_1 (ω) describes how light energy is dispersed from materials, and ε_2 (ω) verifies that light energy is absorbed by materials. The dielectric constant illustrates various optical features like absorption α (ω) and refractive index n (ω) [67].

Fig. 4 (a-d) shows the estimated optical properties in the 0–3.5 eV energy range. The ε_1 (ω) reaches its highest value at corresponding energy of 1.6 eV for Cs_2LiInI_6 and 2 eV for Cs_2NaInI_6, as illustrated in Fig. 4 (a). As energy surpassed resonance value, the value of ε_1 (ω) gradually decreased until it reached its lowest value. By Penn's model $\varepsilon(0) \approx 1 + (\hbar\omega_p/E_g)^2$, the optical band gap ($E_g$) is linked with static ε_1 (0) [68]. It has values between 1.5 and 3 which is highly significant for optoelectronic devices [69]. The response of ε_1 (ω) and n (ω) is similar as shown in Fig. 4 (b), because both exhibit light energy dispersion and material transparency. As seen in Table 1, the expression $n(0) = \sqrt{\varepsilon(0)}$ is well followed by static ε_1 (ω) and n (ω). Fig. 4 (c), the plotted value of ε_2 (ω) represents how materials absorb light. The threshold values of ε_2 (ω) that correspond to the band gap using band structure, can be used to calculate the optical band gap. The light absorption in the visible spectral range is ensured by absorption bands at 2.2 eV and 2.7 eV. The absorption band moves to higher energy when Li is replaced with Na [70]. A different scale, designated by α (ω), can also be used to express light energy absorption, as illustrated in Fig. 4 (d).

Extinction coefficient changed in similar manner as that of ε_2 (ω) as seen in Fig. 5 (a). It is connected with the absorption coefficient (α) as: $\alpha = 4\pi k/\lambda$. The peaks of k (ω) and ε_2 (ω) can be utilized to determine bandgap values. Any material's surface will absorb some of the incident light from a beam of photons when it strikes it at a particular frequency, which will cause the interband transition of electrons to start. The optical conductivity σ (ω) value as depicted in Fig. 5 (b), is used to estimate this transition. Here, we observe peaks at various energy values. The peak value for Cs_2LiInI_6 is 0.4 ($10^8/\Omega$ cm) is seen at 2.3 eV and the peak value for Cs_2NaInI_6 is 0.36 ($10^8/\Omega$ cm) observed at 2.8 eV. Any material used in optoelectronic appliances should contain the greatest value in visible region that is 1.4–4.0 eV, in order to be used in practical applications. Additionally, R (ω) evaluated and presented in Fig. 5 (c) quantifies the reflection and scattering of light by materials. At zero energy, the values for the R (0) are 0.104 and 0.092 for Cs_2LiInI_6 and Cs_2NaInI_6, respectively. Its highest values in the visible range are reported to be 0.105 for Cs_2LiInI_6 and 0.121 for Cs_2NaInI_6 which are incredibly less and confirm the dependability of materials for device applications.

Moreover, L (ω) which is represented in Fig. 5 (d), can be used to evaluate the loss of light energy because of the heating of materials and scattering of light. Its maximum reported value for Cs_2LiInI_6 and Cs_2NaInI_6 is 0.07 and 0.058, respectively. As a result, the investigation of optical characteristics reveals that the maximum visible absorption is significant for optoelectronics.

3.5. Thermoelectric characteristics

Among the most important factors in determining a material's ability to harvest energy is its bandgap, which specifies its position in energy storage devices [71]. The capacity of thermoelectric materials to transform waste thermal energy into electrical energy has received great interest in recent times. The BoltzTrap code included in the WIEN2k package can be utilized to theoretically compute the thermoelectric parameters of any material. Thermoelectric factors including electrical conductivity (σ), thermal conductivity (κ), Seebeck coefficient (S), and power factor (PF) are plotted in Fig. 6 (a-d), whereas the figure of merit (ZT) and lattice thermal conductivity (κ_L) is represented in Fig. 7 (a, b) [72].

Where τ represents relaxation time, for the majority of semiconductors ranging from $10^{-13} - 10^{-14}$ s. In the current study, we used about 10^{-14} s value. High σ and S with a low κ_e values are needed for an ideal thermoelectric material. The plot of σ against temperature range of 200–800 K are presented in Fig. 6 (a). At 200 K, the value of σ seems as 0.34×10^5 ($\Omega^{-1}m^{-1}$) and 0.32×10^5 ($\Omega^{-1}m^{-1}$) for Cs_2LiInI_6 and Cs_2NaInI_6, respectively. So when the temperature is raised to 800 K, the values of σ for both compositions increase linearly up to 1.22×10^5 ($\Omega^{-1}m^{-1}$). The rising carrier concentration, which indicates the semiconducting character of such type of DPs, is responsible for the continuous rise in the σ value. Plotting κ versus temperature demonstrates a similar rising trend to that of σ, κ actually has an electronic (κ_e) and a

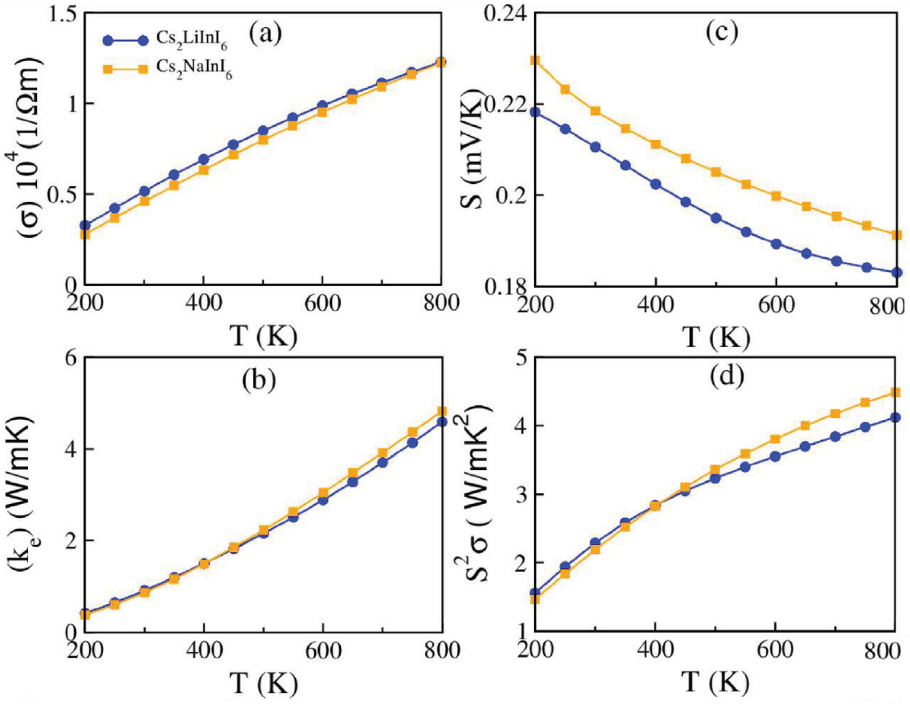

Fig. 6. (a–d): (a) electrical conductivity, (b) electronic part of thermal conductivity, (c) Seebeck coefficient and (d) power factor of Cs_2XInI_6 (X = Li, Na) double perovskites.

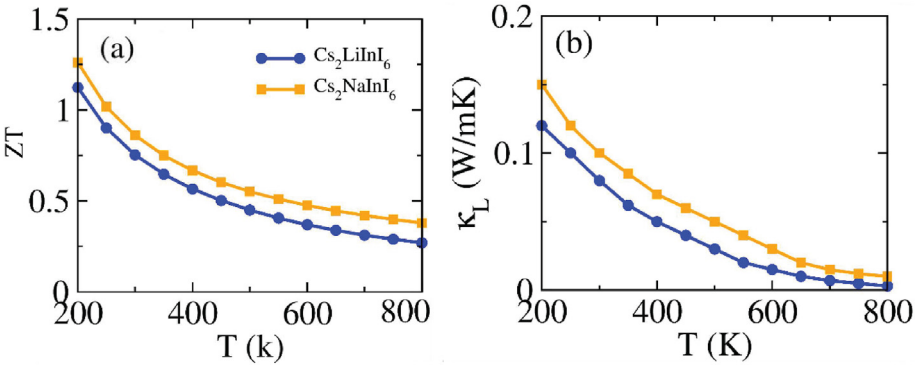

Fig. 7. (a, b): (a) figure of merit and (b) lattice part of thermal conductivity of Cs_2XInI_6 (X = Li, Na) double perovskites.

thermal (κ_l) part. BoltzTrap code can take into account the electronic component, which is shown in Fig. 6 (b) [73]. Furthermore, Wiedemann Franz law (κ_e/σ) can be used to evaluate the supporting role of electrical and thermal involvement in the thermoelectric efficiency of a material. For thermoelectric functioning, the requirement for conductivity is that the thermal conductivity must be lowr than the electrical conductivity and our calculated ratio is 10^{-6} that verifies this condition. Another important factor that is utilized to analyze thermoelectric materials is the Seebeck coefficient. As a result of the temperature gradient (ΔT) around the conductor's ends, it calculates the potential difference (ΔV). The type of charge carriers, such as + ve for holes and -ve for electrons, is determined by the positive (+ve) and negative (-ve) signs of the Seebeck coefficient (S). Seebeck coefficient (S) may be calculated using the Pisarenko relation because PDOS demonstrated the role of the individual states in the development of conduction and valence bands [74].

$$S = 8\pi^2 k_B m^* T\left(3eh^2\right)^{-1}\left(\frac{\pi}{3p}\right)^{2/3} \tag{8}$$

Where k_B represents Boltzmann constant, m* denotes the effective mass of charge carriers, e is the charge on charge carriers, h is Plank's constant, ρ represents carrier concentration and T stands for absolute temperature. As can be seen in Fig. 6 (c), the value of the Seebeck coefficient (S) is observed to decrease as temperature rises. In addition, as the temperature rises, the value of the Seebeck coefficient (S) decreases because the potential difference across the conductor's ends decreases as the ratio of σ/τ rises. The value of the Seebeck coefficient (S) should be more than 200 μV/K for optimal thermoelectric performances. For the current investigation, at 200 K Seebeck coefficient (S) the value of S is given as 219 for Cs_2LiInI_6 and 230 μV/K for Cs_2NaInI_6 composition and at 800 K reduced to 182 and 195 μV/K, respectively [75]. These values illustrate how valuable these compositions could be for thermoelectric systems. Furthermore, because of the existence of bipolar conduction in the material, the value of the Seebeck coefficient (S) decreases as temperature rises. As illustrated in Fig. 6 (d), a different parameter named thermoelectric power factor ($S^2\sigma$), rises with temperature linearly and can be used to evaluate the efficiency of thermoelectric material without the contribution of κ_e. At 200 K, the value of power factor was approximately 1.5 W/mK^2 and 1.6 W/mK^2 for Cs_2LiInI_6 and Cs_2NaInI_6, respectively and then these values increased to 3.9 W/mK^2 for Li based composition and

4.3 W/mK^{2}for Na based composition at 800 K.

The most significant parameter used to evaluate the execution of thermoelectric appliances is the figure of merit (ZT). The ZT is computed utilizing other factors, plotted versus temperature as seen in Fig. 7 (a). At 200 K and 800 K, the measured ZT reduced from 1.23 to 0.25 for Cs_2LiInI_6 and 1.25 to 0.35 for Cs_2NaInI_6. We anticipated that this theoretical report will offer a solid foundation for experimentalists researching thermoelectric devices because the value of the figure of merit (ZT) at RT is approximately 0.75. In thermal conductivity, the role of lattice vibration is shown by κ_L that is individually estimated and plotted in Fig. 7 (b). The low value of κ_L in both compositions ensures, its participation is minimal, which is beneficial for the excellent efficiency of materials. At 200 K, the value of κ_L for Cs_2LiInI_6 and Cs_2NaInI_6 was reported to be 0.13 and 0.15 W/mK, respectively however, these values later dropped to 0.01 W/mK for Cs_2LiInI_6 and 0.02 W/mK for Cs_2NaInI_6 at 800 K, emphasizing the significance of these compositions for potential thermoelectric applications [76].

4. Conclusion

In nutshell, the structural, electronic, mechanical as well as optical and thermoelectric properties of Cs_2XInI_6 (X = Li, Na) are investigated for future usage in applications involving renewable energy. The thermal stability and structural stability of double perovskites are confirmed by the negative formation energy and tolerance factor (0.92–0.90). In the visibl region, the absorption bands are noticed that have potential significance for optoelectronic devices and solar cells. In the most intensely absorbing range, it is reported that the scattering loss and light energy dispersion are at their lowest values. In addition, it is observed that the κ_l is incredibly low, associated with a significant ZT at RT. The investigated double perovskites are hard, ductile, and have high Debye temperatures. These proeprties make these compositions viable for the fabrication of optoelectronic and thermoelectric devices.

CRediT authorship contribution statement

Tariq M. Al-Daraghmeh: Conceptualization. **Omar Zayed:** Conceptualization. **Sadaf Saba:** Formal analysis. **Ghulam M. Mustafa:** Formal analysis. **Othman Hakami:** Formal analysis. **Hind Albalawi:** Supervision. **Z. Mahmoud:** Formal analysis. **Q. Mahmood:** Supervision.

Declaration of competing interest

The authors declare that they have no known competing financial interests or personal relationships that could have appeared to influence the work reported in this paper.

Data availability

Data will be made available on request.

Acknowledgement

This research was funded by the Princess Nourah bint Abdulrahman University Researchers Supporting Project number (PNURSP2023R29), Princess Nourah bint Abdulrahman University, Riyadh, Saudi Arabia. The authors extend their appreciation to the Deanship of Scientific Research at King Khalid University (KKU) for funding this research project Number (RGP.1/44/43)

References

[1] H. Albalawi, G.M. Mustafa, S. Saba, N.A. Kattan, Q. Mahmood, H.H. Somaily, M.A. Amin, Study of optical and thermoelectric properties of double perovskites Cs_2KTlX_6 (X= Cl, Br, I) for solar cell and energy harvesting, Mater. Today Commun. 32 (2022), 104083.

[2] T. Zelai, S.A. Rouf, Q. Mahmood, S. Bouzgarrou, M.A. Amin, A.I. Aljameel, T. Ghrib, H.H. Hegazy, A. Mera, First-principles study of lead-free double perovskites Ga_2PdX_6 (X = Cl, Br, and I) for solar cells and renewable energy, J. Mater. Res. Technol. 16 (2022) 631–639.

[3] M.A. Amin, G. Nazir, Q. Mahmood, J. Alzahrani, N.A. Kattan, A. Mera, et al., Study of double perovskites X_2InSbO_6 (X = Sr, Ba) for renewable energy; alternative of organic-inorganic perovskites, J. Mater. Res. Technol. 18 (2022) 4403–4412.

[4] T.I. Al-Muhimeed, A. Shafique, A.A. AlObaid, M. Morsi, G. Nazir, M.M. Al-Anazy, Q. Mahmood, New lead-free double perovskites X_2GeI_6 (X = K, Rb, Cs) for solar cells, and renewable energy as an alternate of hybrid perovskites, Int. J. Eng. Research 45 (2021) 19645–19652.

[5] A.U. Haq, G.M. Mustafa, M. Amin, S.M. Ramay, A. Mahmood, Ab-initio study of opto-electronic and thermoelectric properties of direct bandgap double perovskites Rb_2XGaBr_6 (X = Na, K), Int. J. Energy Res. 45 (6) (2021) 9241–9251.

[6] L.A. Muscarella, L.A. Muscarella, Halide double-perovskite semiconductors beyond photovoltaics, ACS Energy Lett. 7 (2022) 2128–2135.

[7] I.A. Ajia, P.R. Edwards, Z. Liu, J.C. Yan, R.W. Martin, I.S. Roqan, Excitonic localization in AlN-rich $Al_xGa_{1-x}N/Al_yGa_{1-y}N$ multi-quantum-well grain boundaries, Appl. Phys. Lett. 105 (12) (2014), 12211.

[8] Y. Pak, S. Mitra, N. Alaal, B. Xin, S. Lopatin, D. Almalawi, J.W. Min, H. Kim, Dark-current reduction accompanied photocurrent enhancement in p-type MnO quantum-dot decorated n-type, Appl. Phys. Lett. 116 (11) (2020), 112102.

[9] B. Xin, N. Alaal, S. Mitra, A. Subahi, Y. Pak, D. Almalawi, N. Alwadai, Identifying carrier behavior in ultrathin indirect-bandgap $CsPbX_3$ nanocrystal films for use in UV/Visible-Blind, Small 16 (43) (2020), 2004513.

[10] S. Mitra, Y. Pak, N. Alaal, M.N. Hedhili, D.R. Almalawi, N. Alwadai, Novel P-type wide bandgap manganese oxide quantum dots operating at deep UV range for optoelectronic, Adv. Opt. Mater. 7 (21) (2019), 1900801.

[11] S.A. Khandy, D.C. Gupta, Magneto-electronic, mechanical, thermoelectric and thermodynamic properties of ductile perovskite Ba_2SmNbO_6, Mater. Chem. Phys. 239 (2020), 121983.

[12] F. Qian, M. Hu, J. Gong, C. Ge, Y. Zhou, J. Guo, J. Feng, Enhanced thermoelectric performance in lead-free inorganic $CsSn_{1-x}Ge_xI_3$ perovskite semiconductors, J. Phys. Chem. C 124 (22) (2020) 11749–11753.

[13] R.L. Medeiros, V.R. Melo, D.M. Melo, H.P. Macedo, G.T. Moure, I. Adánez-Rubio, J. Adanez, Double perovskite $(La_{2-x}Ca\text{-}Ba_x)$ NiO_4 oxygen carriers for chemical looping reforming applications, Int. J. Hydrogen Energy 45 (3) (2020) 1681–1696.

[14] Q. Mahmood, G.M. Mustafa, M. Morsi, H. Albalawi, T.H. Flemban, M. Hassan, T. Ghrib, Theoretical investigations of optoelectronic and thermoelectric properties of halide based double perovskite halides: K_2TeX_6, Phys. Scripta 96 (7) (2021), 075703.

[15] A. Kojima, K. Teshima, Y. Shirai, T. Miyasaka, Organometal halide perovskites as visible-light sensitizers for photovoltaic cells, J. Am. Chem. Soc. 131 (17) (2009) 6050–6051.

[16] NREL, Best Research-Cell Efficiency Chart, 2022.

[17] M. Roknuzzaman, K.K. Ostrikov, K.C. Wasalathilake, C. Yan, H. Wang, T. Tesfamichael, Insight into lead-free organic-inorganic hybrid perovskites for photovoltaics and optoelectronics: a first-principles study, Org. Electron. 59 (2018) 99–106.

[18] P. Zhang, J. Yang, S.H. Wei, Manipulation of cation combinations and configurations of halide double perovskites for solar cell absorbers, J. Mater. Chem. 6 (2018) 1809–1815.

[19] M. Sajjad, Q. Mahmood, N. Singh, J.A. Larsson, Ultralow lattice thermal conductivity in double perovskite Cs_2PtI_6: a promising thermoelectric material, ACS Appl. Energy Mater. 3 (11) (2020) 11293–11299.

[20] N.H. Alotaibi, G.M. Mustafa, N.A. Kattan, Q. Mahmood, H. Albalawi, M. Morsi, M.A. Amin, DFT study of double perovskites Cs_2AgBiX_6 (X= Cl, Br): an alternative of hybrid perovskites, J. Solid State Chem. 313 (2022), 123353.

[21] A.H. Slavney, T. Hu, A.M. Lindenberg, H.I. Karunadasa, A bismuth-halide double perovskite with long carrier recombination lifetime for photovoltaic applications, J. Am. Chem. Soc. 138 (7) (2016) 2138–2141.

[22] G. Volonakis, A.A. Haghighirad, R.L. Milot, W.H. Sio, M.R. Filip, B. Wenger, F. Giustino, $Cs_2InAgCl_6$: a new lead-free halide double perovskite with direct band gap, J. Phys. Chem. Lett. 8 (4) (2017) 772–778.

[23] J. Kangsabanik, V. Sugathan, A. Yadav, A. Yella, A. Alam, Double perovskites overtaking the single perovskites: a set of new solar harvesting materials with much higher stability and efficiency, Physical Review Materials 2 (5) (2018), 055401.

[24] S. Chakraborty, W. Xie, N. Mathews, M. Sherburne, R. Ahuja, M. Asta, S.G. Mhaisalkar, Rational design: a high-throughput computational screening and experimental validation methodology for lead-free and emergent hybrid perovskites, ACS Energy Lett. 2 (4) (2017) 837–845.

[25] H. Wang, W. Su, J. Liu, C. Wang, Recent development of n-type perovskite thermoelectrics, Journal of Materiomics 2 (3) (2016) 225–236.

[26] H. Li, L. Tian, Z. Shi, Y. Li, C. Li, J. Feng, H. Zhang, Double perovskite $Cs_2NaInCl_6$ nanocrystals with intense dual-emission via self-trapped exciton-to-Tb^{3+} dopant energy transfer, J. Mater. Chem. C 10 (2022) 10609–10615.

[27] L. Chen, W. Yang, H. Fu, L. Wenna, G. Shao, B. Tang, Mn^{2+}-doped $Cs_2NaInCl_6$ double perovskites and their photoluminescence properties, J. Mater. Sci. 56 (2021) 8048–8059.

[28] B. Zhou, Z. Liu, S. Fang, H. Zhong, B. Tian, Y. Wang, H. Li, Efficient white photoluminescence from self-trapped excitons in Sb^{3+}/Bi^{3+} Co-doped $Cs_2NaInCl_6$ double perovskites with tunable dual-emission, ACS Energy Lett. 6 (9) (2021) 3343–3351.

[29] Z. Shuai, Y. Kumiko, I. Satoshi, H. Shuzi, M. Tingli, First-principles study of electronic and optical properties of lead-free double perovskites Cs_2NaBX_6 (B = Sb, Bi; X = Cl,, Br, I) 117 (2018) 117–121.

[30] H.H. Hegazy, G.M. Mustafa, A. Nawaz, N.A. Noor, A. Dahshan, I. Boukhris, Tuning of direct bandgap of Rb_2ScTlX_6 (X= Cl, Br, I) double perovskites through halide ion substitution for solar cell devices, J. Mater. Res. Technol. 19 (2022) 1271–1281.

[31] S.V. Trukhanov, I.O. Troyanchuk, M. Hervieu, H. Szymczak, K. Bärner, Magnetic and electrical properties of LBaMn2O6-γ (L = Pr, Nd, Sm, Eu, Gd, Tb) manganites, Phys. Rev. B 66 (2002), 184424-10.

[32] I.Z. Zhumatayeva, I.E. Kenzhina, A.L. Kozlovskiy, M.V. Zdorovets, The study of the prospects for the use of $Li_{0.15}Sr_{0.85}TiO_3$ ceramics, J. Mater. Sci. Mater. Electron. 31 (2020) 6764–6772.

[33] A.V. Trukhanov, L.V. Panina, S.V. Trukhanov, V.A. Turchenko, M. Salem, Evolution of structure and physical properties in Al-substituted Ba-hexaferrites, Chin. Phys. B 25 (2016) 16102–16106.

[34] M.V. Zdorovets, A.L. Kozlovskiy, D.I. Shlimas, D.B. Borgekov, Phase transformations in FeCo - Fe_2CoO_4/Co_3O_4-spinel nanostructures because of thermal annealing and their practical application, J. Mater. Sci. Mater. Electron. 32 (2021) 16694–16705.

[35] T.I. Zubar, S.A. Sharko, D.I. Tishkevich, N.N. Kovaleva, D.A. Vinnik, S.A. Gudkova, E.L. Trukhanova, E.A. Trofimov, S.A. Chizhik, L.V. Panina, S.V. Trukhanov, A.V. Trukhanov, Anomalies in Ni-Fe nanogranular films growth, J. Alloys Compd. 748 (2018) 970–978.

[36] A.L. Kozlovskiy, M.V. Zdorovets, Synthesis, structural, strength and corrosion properties of thin films of the type CuX (X = Bi, Mg, Ni), J. Mater. Sci. Mater. Electron. 30 (2019) 11819–11832.

[37] S.V. Trukhanov, I.O. Troyanchuk, A.V. Trukhanov, I.M. Fita, A.N. Vasil'ev, A. Maignan, H. Szymczak, Magnetic properties of $La_{0.70}Sr_{0.30}MnO_{2.85}$ anion-deficient manganite under hydrostatic pressure, J. Exp. Theor. Phys. Lett. 83 (2006) 33–36.

[38] A. Kozlovskiy, K. Egizbek, M.V. Zdorovets, M. Ibragimova, A. Shumskaya, A.A. Rogachev, Z.V. Ignatovich, K. Kadyrzhanov, Evaluation of the efficiency of detection and capture of manganese in aqueous solutions of FeCeOx nanocomposites doped with Nb2O5, Sensors 20 (2020) 4851.

[39] D.A. Vinnik, A.Yu Starikov, V.E. Zhivulin, et al., Structure and magnetodielectric properties of titanium substituted barium hexaferrites, Ceram. Int. 47 (2021) 17293–17306.

[40] V.A. Turchenko, S.V. Trukhanov, V.G. Kostishin, F. Damay, et al., Impact of In3+ cations on structure and electromagnetic state of M-type hexaferrites, J. Energy Chem. 69 (2022) 667–676.

[41] S.V. Trukhanov, V.V. Fedotova, A.V. Trukhanov, S.G. Stepin, H. Szymczak, Synthesis and structure of nanocrystalline $La_{0.50}Ba_{0.50}MnO_3$, Crystallogr. Rep. 53 (2008) 1177–1180.

[42] A. Kozlovskiy, I. Kenzhina, Z.A. Alyamova, M. Zdorovets, Optical and structural properties of AlN ceramics irradiated with heavy ions, Opt. Mater. 91 (2019) 130–137.

[43] A. Jain, S.P. Ong, G. Hautier, W. Chen, W.D. Richards, S. Dacek, S. Cholia, D. Gunter, D. Skinner, G. Ceder, K.A. Persson, The Materials Project: a materials genome approach to accelerating materials innovation, Apl. Mater. 1 (1) (2013), 011002.

[44] S. Nazir, N.A. Noor, M. Manzoor, A. Dahshan, Ab-initio simulations of Li-based double perovksites $A_2LiInBr_6$ (A = Rb, Cs) for solar cell applications, Chem. Phys. Lett. 798 (2022), 139612.

[45] M. Manzoor, M. Waqas Iqbal, M. Imran, N.A. Noor, A. Mahmood, Y.M. Alanazi, S. Aftab, Probing direct bandgap of double perovskites Rb2LiTlX6 (X ¼ Cl, Br) and optoelectronic characteristics for Solar cell applications: DFT calculations, J. Mater. Res. Technol. (2022) 4775–4785.

[46] S. Iqbal, G.M. Mustafa, M. Asghar, N.A. Noor, M. Waqas Iqbal, A. Mahmood, Y.H. Shin, Tuning the optoelectronic and thermoelectric characteristics of narrow bandgap Rb_2AlInX_6(X= Cl, Br, I) double perovskites: a DFT study, Mater. Sci. Semicond. Process. 143 (2022), 106551.

[47] V.B. Bobrov, S.A. Trigger, On the problem of universal density functional, Bull. Lebedev Phys. Inst. 45 (4) (2018) 127–130.

[48] P. Blaha, K. Schwarz, F. Tran, R. Laskowski, G.K. Madsen, L.D. Marks, WIEN2k: an APW+ lo program for calculating the properties of solids, J. Chem. Phys. 152 (7) (2020), 074101.

[49] J.P. Perdew, K. Burke, M. Ernzerhof, Generalized gradient approximation made simple, Phys. Rev. Lett. 77 (18) (1996) 3865.

[50] F. Tran, P. Blaha, Accurate band gaps of semiconductors and insulators with a semilocal exchange-correlation potential, Phys. Rev. Lett. 102 (22) (2009), 226401.

[51] T.I. Al-Muhimeed, A.I. Aljameel, A. Mera, S. Saad, G. Nazir, H. Albalawi, Q. Mahmood, First principle study of optoelectronic and mechanical properties of lead-free double perovskites Cs_2SeX_6 (X= Cl, Br, I), J. Taibah Univ. Sci. 16 (1) (2022) 155–162.

[52] G.A. Mersal, H. Alkhaldi, G.M. Mustafa, Q. Mahmood, A. Mera, S. Bouzgarrou, M.A. Amin, Study of half metallic ferromagnetism and thermoelectric properties of spinel chalcogenides $BaCr_2X_4$ (X= S, Se, Te) for spintronic and energy harvesting, J. Mater. Res. Technol. 18 (2022) 2831–2841.

[53] W. Li, J. Carrete, N.A. Katcho, N. Mingo, ShengBTE: a solver of the Boltzmann transport equation for phonons, Comput. Phys. Commun. 185 (6) (2014) 1747–1758.

[54] M.T. Anderson, K.B. Greenwood, G.A. Taylor, K.R. Poeppelmeier, B-cation arrangements in double perovskites, Prog. Solid State Chem. 22 (3) (1993) 197–233.

[55] E. Haque, M.A. Hossain, Electronic, phonon transport and thermoelectric properties of $Cs_2InAgCl_6$ from first-principles study, Computational Condensed Matter 19 (2019), e00374.

[56] H. Albalawi, B.U. Haq, G. Nazir, T. Ghrib, N.A. Kattan, Q. Mahmood, A.I. Aljameel, M. Morsih, S. Bouzgarrou, Study of new double perovskite halides $Rb_2Ti(Cl/Br)_6$ for solar cells and thermoelectric applications, Mater. Today Commun. 32 (2022), 104106.

[57] C.J. Bartel, C. Sutton, B.R. Goldsmith, R. Ouyang, C.B. Musgrave, L.M. Ghiringhelli, M. Scheffler, New tolerance factor to predict the stability of perovskite oxides and halides, Sci. Adv. 5 (2) (2019), eaav0693.

[58] O. Hellman, D. Broido, A. Phonon, Thermal transport in Bi_2Te_3 from first principles, Phys. Rev. B 90 (2014), 134309.

[59] J.H. Noh, S.H. Im, J.H. Heo, T.N. Mandal, S.I. Seok, Chemical management for colorful, efficient, and stable inorganic–organic hybrid nanostructured solar cells, Nano Lett. 13 (4) (2013) 1764–1769.

[60] B.B. Karki, G.J. Ackland, J. Crain, Elastic instabilities in crystals from ab initio stress-strain relations, J. Phys. Condens. Matter 9 (41) (1997) 8579.

[61] M. Roknuzzaman, K.K. Ostrikov, H. Wang, A. Du, T. Tesfamichael, Towards lead-free perovskite photovoltaics and optoelectronics by ab-initio simulations, Sci. Rep. 7 (1) (2017) 1–8.

[62] Y.J. Hao, X.R. Chen, H.L. Cui, Y.L. Bai, First-principles calculations of elastic constants of c-BN, Phys. B Condens. Matter 382 (2006) 118–122.

[63] R. Singh, G. Balasubramanian, Impeding phonon transport through superlattices of organic–inorganic halide perovskites, RSC Adv. 7 (59) (2017) 37015–37020.

[64] M. Marathe, A. Grünebohm, T. Nishimatsu, P. Entel, C. Ederer, First-principles-based calculation of the electrocaloric effect in $BaTiO_3$: a comparison of direct and indirect methods, Phys. Rev. B 93 (5) (2016), 054110.

[65] M. Hu, J. He, Q. Wang, Q. Huang, D. Yu, Y. Tian, B. Xu, Covalent-bonded graphyne polymers with high hardness, J. Superhard Mater. 36 (4) (2014) 257–269.

[66] S. Tariq, M.I. Jamil, A. Sharif, S.M. Ramay, H. Ahmad, B. Tahir, Exploring structural, electronic and thermo-elastic properties of metallic $AMoO_3$ (A= Pb, Ba, Sr) molybdates, Appl. Phys. A 124 (1) (2018) 1–8.

[67] R. Anbarasan, M. Srinivasan, R. Suriakarthick, H. Albalawi, J.K. Sundar, P. Ramasamy, Q. Mahmood, Exploring the structural, mechanical, electronic, and optical properties of double perovskites of Cs_2AgInX_6 (X= Cl, Br, I) by first-principles calculations, J. Solid State Chem. 310 (2022), 123025.

[68] D.R. Penn, Wave-number-dependent dielectric function of semiconductors, Phys. Rev. 128 (1962) 2093–2097.

[69] Q. Mahmood, M.H. Alhossainy, M.S. Rashid, T.H. Flemban, H. Althib, T. Alshahrani, A. Laref, First-principles study of lead-free double perovskites Rb_2TeX_6 (X= Cl, Br, and I) for solar cells and renewable energy, Mater. Sci. Eng., B 266 (2021), 115064.

[70] N.A. Noor, Q. Mahmood, M. Rashid, B.U. Haq, A. Laref, The pressure-induced mechanical and optoelectronic behavior of cubic perovskite $PbSnO_3$ via ab-initio investigations, Ceram. Int. 44 (12) (2018) 13750–13756.

[71] W. Li, S. Lin, X. Zhang, Z. Chen, X. Xu, Y. Pei, Thermoelectric properties of Cu_2SnSe_4 with intrinsic vacancy, Chem. Mater. 28 (17) (2016) 6227–6232.

[72] S. Ali, M. Rashid, M. Hassan, N.A. Noor, Q. Mahmood, A. Laref, B.U. Haq, Ab-initio study of electronic, magnetic and thermoelectric behaviors of LiV_2O_4 and $LiCr_2O_4$ using modified Becke-Johson (mBJ) potential, Phys. B Condens. Matter 537 (2018) 329–335.

[73] H.C. Wang, P. Pistor, M.A. Marques, S. Botti, Double perovskites as p-type conducting transparent semiconductors: a high-throughput search, J. Mater. Chem. 7 (24) (2019) 14705–14711.

[74] M. Sajjad, N. Singh, S. Sattar, S. De Wolf, U. Schwingenschlögl, Ultralow lattice thermal conductivity and thermoelectric properties of monolayer Tl_2O, ACS Appl. Energy Mater. 2 (5) (2019) 3004–3008.

[75] A.H. Reshak, S. Auluck, Thermoelectric properties of nowotny–juza NaZnX (X= P, as and Sb) compounds, Comput. Mater. Sci. 96 (2015) 90–95.

[76] X. Ji, Y. Yu, J. Ji, J. Long, J. Chen, D. Liu, Theoretical studies of the pressure-induced phase transition and elastic properties of BeS, J. Alloys Compd. 623 (2015) 304–310.